July 2008 Volume 4 Issue 4

Trade Science Inc.

Materials Science

An Indian Journal

Full Paper

MSAIJ, 4(4), 2008 [335-341]

Oxidation behaviour of aluminium and its alloys in molten $NaNO_3$

S.S.Mahmoud*, M.M.Ahmed, A.A.Kassab, R.A.El-Kasaby

Chemistry Department, University College of Girls for Arts, Science and Education, Ain shams University, Heliopolis, Cairo, (EGYPT)

E-mail: drsohairr@hotmail.com

Received: 16th June, 2008 ; Accepted: 21st June, 2008

ABSTRACT

The oxidation behavior of aluminum and its allays was investigated in molten $NaNO_3$ at 400°C .The techniques of measurements were: open-circuit potential, galvanic current, anodic galvanostatic polarization and electrochemical impedance spectroscopy. The electrodes undergo spontaneous passivation in molten $NaNO_3$ due to the formation of oxide scales on their surface. The thickness of the oxide scales increases with increasing immersion time and also depends on the composition of the electrode. Corrosion tests of the oxide scales formed on the electrodes surface in aqueous HCl solution indicate that these scales dissolve after an induction period with a rate depending on the composition of the electrode. The oxide scales formed during oxidation in molten $NaNO_3$ under anodic polarization conditions are multilayered. The inner layer of oxide scales is more protective than the outer layer.

KEYWORDS

Aluminum alloys
Molten $NaNO_3$;
Oxidation behavior.

INTRODUCTION

Aluminum is the second most widely used metal for industrial purposes[1]. Also aluminum alloys lend themselves to many engineering applications because of their combination of lightness with strength. Alloying of aluminum with different elements in general improves its mechanical and physical properties. Aluminum is often alloyed with silicon and/or copper.

Considerable attention has been paid to oxide film formation, as oxide films allow many important industrial metals and alloys to be used in the environment where they would not have been otherwise stable. In addition, the growth of anodic oxide films on aluminum has been studied extensively, due to their use as capacitor dielectrics. Because the anodic film on aluminum is thin in an alkaline solution, the alkaline electrolytes are used less often than acid electrolytes which are more often used. These include: oxalic acid, phosphoric acid, sulphuric acid, etc. as single-acid electrolytes. Recently, mixed electrolytes such as chromic acid-sulphuric acid, nitric acid-sulphuric acid and boric acid-sulphuric acid have been used for anodic oxide film formation on aluminum[2-5]. Also, neutral solutions of borates, tartrates and some organic acids can be used for anodic oxide film formation on aluminum[6,7].

Molten oxyanion salts are also used as electrolytes for oxide formation on aluminum[8-10]. For this reason the oxidation behavior of aluminum and its alloys in molten sodium nitrate is investigated in the present study.

EXPERIMENTAL

The working electrodes were prepared from cylindrical rods of aluminum and its alloys, having the dimension of 0.7 cm diameter and 6 cm length. These electrodes have the chemical composition shown in TABLE 1 and were supplied from Misr Aluminum Company, Egypt.

Thus before each experiment, the electrodes were

Full Paper

mechanically polished using emery papers of different grades and degreased with acetone. After mechanical polishing, the working electrodes were dipped for few seconds in a pickling bath consisting of concentrated H_2SO_4 (96%)- HNO_3(70%) -HF(46%) mixed in the volume ratio 10:4:3. The electrodes were removed and rinsed several times with distilled water. The $NaNO_3$ melt (AR grade) was prepared and dried as previously described[11,13]. The prepared $NaNO_3$ was kept in a closed desiccator till required.

Experiments were carried out in tall unlipped pyrex glass tubes(5 cm in diameter and 11 cm long). The working vessel was surrounded by a stainless steel container which was placed in an electrically heated crucible-type furnace. The temperature was regulated by using a variable transformer and measured by a Ni /Ni-Cr thermocouple (±2°C). The thermocouple was separated from the melt by tight-fitting pyrex tube.

The potentials of the electrodes were measured relative to a Ag/Ag^+, $NaNO_3$, 2.04% $AgNO_3$ reference electrode[11,13]. A platinum sheet (1.5×1.5 cm) spot welded to a platinum rod was used as an auxiliary electrode and separated from the melt by placing it in special pyrex tube with a medium porosity sintered pyrex disc. The polarization current values were derived from a constant-current unit (DC power supply GP-4303D, LG Precision Co, Korea). The potential and current measurements were performed using a multimeter (model 1008,Kyoritsu Electrical Instruments, Japan) (input impedance 100MΩ). The impedance measurements were carried out using an impedance measurement system (Model 1M6 Zahner Electrik, Meβtechnik, Germany).

The corrosion tests on the oxide scales were carried out in 0.2 M HCl solution using potential-time measurements under open-circuit conditions.

RESULTS AND DISCUSSION

(1) Open-circuit potentials measurements

Corrosion potentials, E_{corr}, of the electrodes (I-V) were measured as a function of time under open-circuit conditions at 400°C. The results are plotted in figure 1. It is clear that E_{corr} shifts to more positive values upon immersion of the electrodes in the nitrate melt and then reaches the steady-state value E_s. The time required for attaining E_s depends on the composition of the alloy

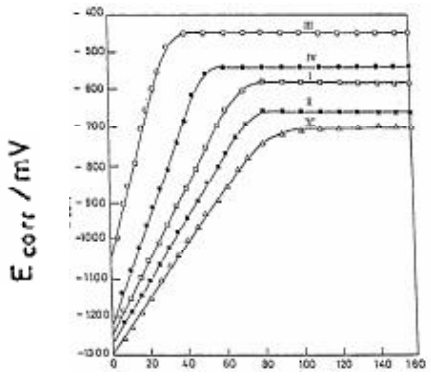

Figure 1: Variation of the corrosion potential with time in molten $NaNO_3$ at 400°C

TABLE 1: Chemical analysis of the working electrodes

Element	Working electrode				
wt%	I	II	III	IV	V
Si	7.040	0.450	8.790	11.050	0.0600
Fe	0.090	0.180	0.130	0.110	0.1600
Cu	0.000	0.001	0.980	0.000	0.0004
Mn	0.004	0.011	0.006	0.005	0.0015
Mg	0.291	0.490	0.360	0.182	0.0010

and decreases according the order: V>II>I>IV>III.

The anodic process may be dissolution and/or anodic barrier layer formation in addition to the solvent. The barrier layer may be formed by a dissolution-precipitation mechanism and /or a solid-state mechanism. In molten nitrates the oxide ions originate by self-dissociation according to the equilibrium:

$$NO_3^- \rightleftharpoons NO_2^+ + O^{2-} \quad (1)$$

In Lux-Flood, acid-base properties of molten oxyanion salts[14-16], NO_2^+ is the acid and O^{2-} is the base. Thus the reactions leading to oxidation of metals, M, in the alloys may be represented by the following equations[11-13].

$$M + n/2\ O^{2-} \rightleftharpoons MO_{n/2} + ne \quad (2)$$

and /or

$$M + n/2\ NO_3^- \rightleftharpoons MO_{n/2} + n/2\ NO_2^+ + ne \quad (3)$$

The formation of the metal oxide on the electrodes surface causes their spontaneous passivation and shifts their potential in the more positive direction. Equations[2,3] represent the anodic path of the electrochemical reaction. The cathodic path can be represented by [11-13]

$$NO_2^+ + e \rightleftharpoons NO_2 \quad (4)$$

In the former process the metal is assumed to dissolve actively until supersaturation is reached, then the metal cations react with the electrolyte to form the barierr

layer as an insulating precipitate on the metal surface. Formation of the oxide can be represented as follows[17].

$$M \xrightarrow{k_d} M^{n+} + ne \quad (5)$$

$$M^{n+} + n/2\ O^{2-} \underset{}{\overset{kf}{\rightleftharpoons}} MO \quad (6)$$

where k_d, k_f,k_{-f} are the rate constants for the metal dissolution, oxide formation and oxide dissolution, respectively. In the present study the aluminum oxide film is sparingly soluble in the melt and hence $k_f >> k_{-f}$.

During oxidation of the electrodes in molten $NaNO_3$ the corrosion potential E_{corr} varies with time t according to the following equation.

$$E_{corr} = k_1 + k_2 \log (t + t^o) \quad (7)$$

where K_1,K_2,t^o are constants for a given electrode. Equation[7] was derived by a number of investigators [17-19] on the basis of oxide growth under high electric fields. The field is assumed to be created by adsorption of anions on the metal oxide surface which creates an image charge of the same magnitude but of opposite sign on the metal surface. Since the positive shift in E_{corr} of electrodes is directly proportional to the oxide film thickness, it may be possible to take k_2 as a measure of the rate of oxide layer thickening per decade of time.

Figure 2 shows that the equation[7] is applicable to the present results for electrodes I-V in molten $NaNO_3$. The plots in figure 2 indicate that for each electrode there are two values for the rate of oxide formation, k_2. The first value is for the initial stages of oxidation and formation of the oxide layer, while the second value is for the thickening of the oxide layer. The first values are lower than the second values. The values of k_2 are calculated from the slopes ($\Delta E_{corr}/\Delta$ log time) of the plots in figure 2 for the electrodes and are listed in TABLE 2. The results in figure 2 and TABLE 2 indicate that the values of k_2 greatly depend on the composition of the electrode.

(2) Anodic polarization measurements

Figure 3 presents the conditions of low anodic polarization where the potential E of the nonlinear part of the Tafel plot against the current density for electrodes I-V at 400°C, Different slopes ($\Delta E/\Delta i = R_p$) are obtained for each electrode. The R_p values are listed in TABLE 3. The different values of exchange current i_o are calculated for the electrodes using the equation.

$$(dE/di)\eta_{=0} = R_p = (RT/ZF\, i_o) \quad (8)$$

where R_p is the polarization resistance of the oxide scales at low polarization conditions, R is the gas constant, T is the temperature, Z is the number of the electrons (Z is taken roughly =3) and F is the Faraday. The calculated values of i_o are listed in TABLE 3. The results of this TABLE indicate that the value of R_p increases in the order V < II < I < IV < III. The values of i_o decrease in the same order.

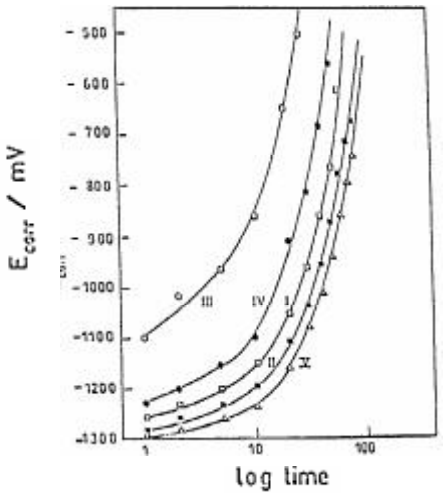

Figure 2: Variation of corrosion potential, E_{corr}, of the electrodes with log time in pure nitrate melt at 400°C

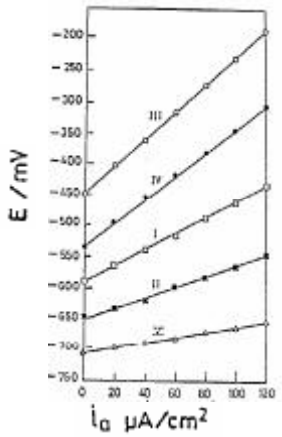

Figure 3: Plots of E with i_a at low polarization conditions for electrodes in molten $NaNO_3$ at 400°C

TABLE 2: Open-circuit measurements for the electrodes in molten $NaNO_3$ ss at 400°C

	I	II	III	IV	V
E_s/ mV	-580	-660	-450	-540	-700
t_s/ min	75	86	40	53	90
$1^{st}k_2$ mV/decade	110	90	250	125	75
$1^{st}k_2$ mV/ decade	571.42	500	850	785	392.85

Figure 4 represents the galvanostatic anodic polarization behavior of electrodes I-V immersed in molten $NaNO_3$ at 400°C. After reaching steady-state potential under open-circuit conditions, the potential first increases slowly with increase of applied current density, then greatly increases with increasing of current density, indicating the onset of definite passivation. This type of passivation occur at definite current density, the pas-

Full Paper

TABLE 3: Galvanostatic anodic polarization measurements for the electrodes in molten $NaNO_3$ at 400°C

	I	II	III	IV	V
R_p / Ω	1250	875	2222.2	1875	500
i_o /μA cm^{-2}	15.435	22.05	8.682	10.290	38.589
i_{corr} /μA cm^{-2}	20	30	8.5	10	85
i_p /μA cm^{-2}	200	500	75	100	700

TABLE 4: Galvanic current measurements for the electrodes in molten $NaNO_3$ at 400°C

Electrode	i_{imm} /μA	i_s/μA	i_{imm}- i_s/μA	t_s /min
I	750	25	725	70
II	760	50	710	90
III	740	5	735	30
IV	750	20	730	50
V	760	75	685	100

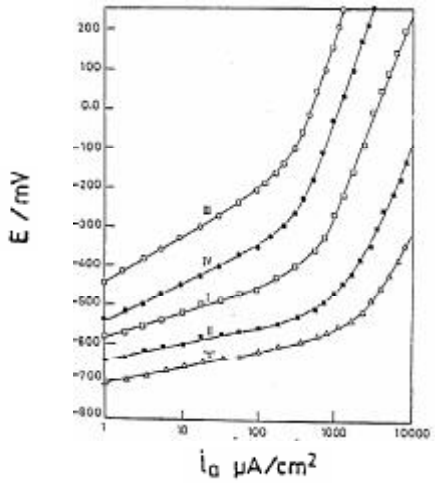

Figure 4: Galvanostatic anodic polarization curves for electrodes

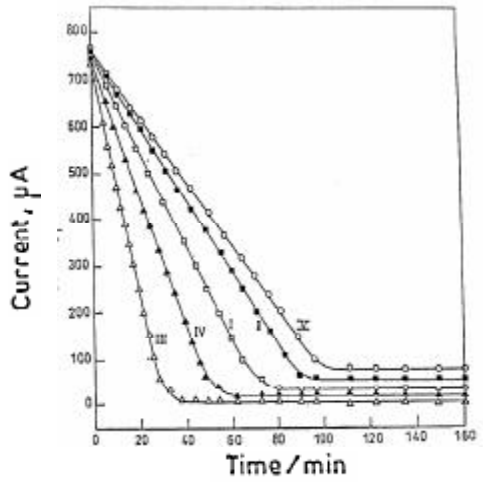

Figure 5: Galvanic current-time plots for the electrodes in nitrate melt at 400°C

sivation current density i_p. The corrosion current density i_{corr} for the electrodes was determined by extrapolating the linear portion of the Tafel plot to zero overvoltage (η=0), where η equals the difference between the polarization patential and the open-circuit potential. Also, the value of passivation current density can be determined by extrapolating the vertical part of the polarization curves to zero overvoltage (η=0) as above mentioned. The values of i_{corr} and i_p are listed in TABLE 3. The results indicate that the values of i_{corr} and i_p greatly depend on the chemical composition of the electrodes.

(3) Galvanic current measurements

For the investigation of the oxidation behavior of the electrodes, the galvanic current between electrode and the inert Pt electrode was measured until the steady state was reached[20-22].

Figure 5 represents the galvanic current-time plots of the electrodes. The plots indicate that upon immersion of the electrodes in the melt, the galvanic current greatly decreases with time until reaching steady-state values. The time required to reach the steady state (t_s) depends on the composition of the electrode and decreases according to the order V > II > I > IV > III.

The values of the galvanic current at the moment of electrode immersion in the melt (i_{imm}) and at the steady state (i_s) and the difference (i_{imm}-i_s) are deduced from the plots in figure 5 and are listed in TABLE 4. If we roughly consider the value of i_{imm}-i_s as a measure of thickness and protective properties of oxide scales, this means these properties depend on the chemical composition of the electrodes. Also, these results indicate that the electrodes surface passivates and the passive layer protects the electrodes from continuous corrosion.

(4) Electrochemical impedance measurements

The electrochemical impedance spectroscopy (EIS) is powerful tool in the investigation of corrosion and passivation phenomena in aqueous and non-aqueous media[21-26].

The impedence characteristics of the electrodes in molten $NaNO_3$ were measured under open-circuit conditions after reaching the steady-state potential at 400°C. Figure 6 presents the impedance diagrams (Nyqiust plots) for the electrodes at steady-state conditions. These impedance diagrams are not perfect semicircles, which has been attributed to frequency dispersion[27,28]. In real systems, e.g. corrosion, the deviation from the ideal semicircles exists corresponding to rotation of center of the capacitive loop by angle Φ below

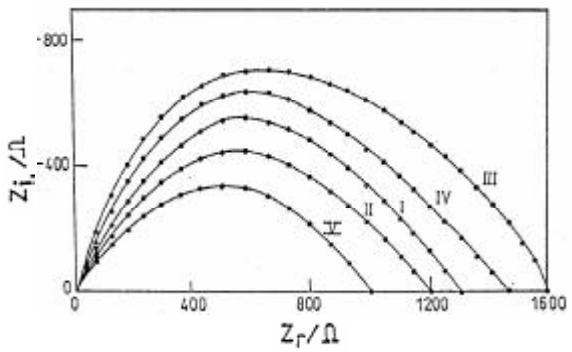

Figure 6: Nyquist plots for electrodes in molten $NaNO_3$ measured after reaching the steady-state potential under open- circuit conditions at 400°C

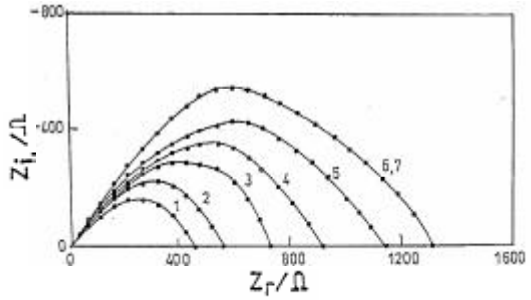

Figure 7: Nyquist plot for electrode I at different immersion times: (1)15 min, (2)30 min, (3)40 min, (4)50 min, (5)60 min, (6)70 min, (7)80 min

the real axis.

Deviation of this kind often referred to frequency dispersion, which has been attributed to inhomogeneties of the solid surfaces[29-30] the charge transfer resistance (R_p) values are calculated from the difference in impedance at lower and higher frequencies[31].The double layer capacitance C_{dl} was determined from the frequency f at which Z_i is maximum, using the relationship.

$$-f Z_{i,max} = (2\pi C_{dl} R_p)^{-1} \quad (9)$$

The derived impedance parameters are given in TABLE 5. These results indicate that the value of R_p depends on the composition of the electrode and increases in the order V < II < I < IV < III, while the value of C_{dl} decreases in the same order. The values of R_p and C_{dl} give an indication of the thickness of the oxide scales formed on the electrodes surface. The more thick the oxide scales, the higher the values of R_p and the lower the values of C_{dl}. These results are in a good agreement with the previously obtained by other techniques.

The thickening of oxide scales on the electrode surfaces can be followed by impedance measurements,

TABLE 5: Impedance measurements for the electrodes in molten $NaNO_3$ at 400°C

Electrode	R_p /Ω.cm^2	C_{dl} /μF. cm^{-2}
I	1300	2.23
II	1200	2.95
III	1600	1.42
IV	1450	1.69
V	1000	4.50

TABLE 6: Impedance data for electrodes I-V in molten $NaNO_3$ at 400°C at different immersion times

Electrode I			Electrode II		
Time/ min	R_p/Ω.cm^2	C_{dl}/μF.cm^{-2}	Time/min	R_p/Ω.cm^2	C_{dl}/μF.cm^{-2}
15	470	22.59	20	475	22.3
30	550	13.16	40	575	13.85
40	725	7.85	60	740	7.69
50	900	4.72	80	1000	4.55
60	1120	3.35	90	1200	2.95
70	1300	2.23	100	1200	2.95
80	1300	2.23			
Electrode III			**Electrode IV**		
Time/min	R_p/Ω.cm^2	C_{dl}/μF.cm^{-2}	Time/min	R_p/Ω.cm^2	C_{dl}/μF.cm^{-2}
5	460	13.31	10	550	14.48
10	650	8.60	20	675	7.86
15	820	6.07	30	900	4.72
20	1110	3.59	40	1220	2.75
25	1350	2.41	50	1450	1.69
30	1600	1.42	60	1450	1.69
40	1600	1.42			

Electrode V		
Time/min	R_p/Ω.cm^2	C_{dl}/μF. cm^{-2}
20	425	26.76
40	550	14.48
60	700	10.11
80	850	6.69
100	1000	4.50
120	1000	4.50

where the Nyquist plots are presented as functions of immersion time in molten $NaNO_3$ under open-circuit conditions at 400°C, as shown in figure 7 for the electrode I. Similar Nyquist plots are obtained for the other electrodes but not shown. The plots are depressed semicircles, the diameters of which increase with immersion time until the steady state is reached. This indicates that the polarization resistance of the oxide layer increases with increase of immersion time since this capacitive semicircle is correlated with the dielectric properties and thickness of the barrier oxide film[30] the values R_p and C_{dl} for the electrodes are calculated as mentioned above and are listed in TABLE 6 for different immersion times. These results indicate that the value of R_p increases with increase of immersion time until steady state is reached. On the other hand, the value of C_{dl} decreases with increase of immersion time. These results indicate the formation of protective passive oxide

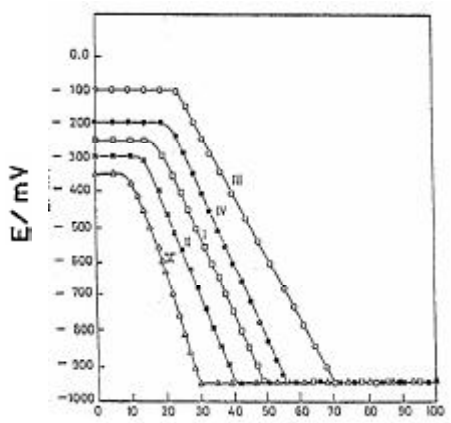

Figure 8: Potential-time curves for electrodes in 0.2M HCl after oxidation in molten $NaNO_3$ at 400°C under open-circuit conditions

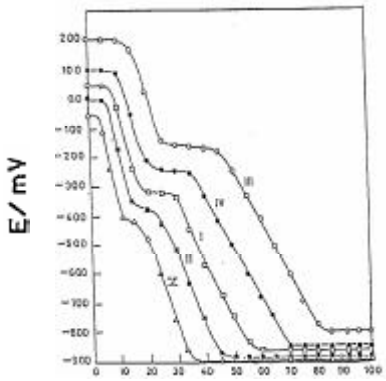

Figure 9: Potential-time curves for electrodes in 0.2M HCl after oxidation in molten $NaNO_3$ at 400°C under polarization conditions

scales on the electrodes surface upon their immersion in molten $NaNO_3$.

(5) Corrosion tests on the oxide scales

Figure 8 presents the potential-time curves for the electrodes when immersed in 0.2M aqueous HCl solutions after having been oxidized under open-circuit conditions in molten $NaNO_3$ at 400°C.

The curves in figure 8 indicate that on immersion of the preoxidized electrodes in HCl solution there is an induction period after which the potential of the electrodes shifts in the active direction before reaching a steady-state condition. The time of the induction period and the time required to reach the steady-state condition depend the composition of the electrodes. These values were determined from the plots of figure 8 and are listed in TABLE 7.

Considering the immersion potential (E_{imm}, the electrode potential at the moment of its immersion in HCl

TABLE 7: Corrosion data for oxide scales on preoxidised electrodes under open-circuit conditions

	I	II	III	IV	V
Induction period /min	17	14	25	20	10
E_{imm}/ mV	-250	-300	-100	-200	-350
E_s/ mV	-950	-950	-950	-950	-950
E_{imm}- Es / mV	700	650	850	750	600
Time of dissolution/min	32	25	45	36	20
mV/ min	22	26	18.9	21	30

TABLE 8: Corrosion data for oxide scales on preoxidised electrodes under galvanostatic anodic polarization conditions

	I	II	III	IV	V
1st step					
Induction eriod/min	7	5	12	9	3
E_{imm}/mV	50	0.00	200	100	-50
E_s/mV	-325	-350	-150	-250	-400
(E_{imm}-E_s)/mV	375	350	350	350	350
Dissolution time/min	13	10	18	15	8
Rate of dissolution m/min	28.8	35	19.4	23.3	43.75
2nd step					
Induction eriod/min	10	7	20	11	6
E_s/mV	-860	-880	-800	-850	-900
Dissolution time/min	27	25	35	30	18
(E_{imm}-E_s)/mV	535	510	650	600	450
Rate of dissolution V/min	19.8	4	18.57	20	25

solution) as the starting potential for the preoxidized electrode and the steady-state potential (E_s) as the final potential, the value E_{imm}-E_s (dissolution potential range) can be calculated. The time required for the shift in potential from E_{imm} to E_s to take place t_s is recorded. The rate of dissolution of the oxide scales can be estimated by dividing the value of E_{imm}-E_s by t_s [12,13,19]. The calculated results listed in TABLE 7 indicate that the values of E_{imm} and the rate of dissolution depend on the composition of the electrodes. The rate of dissolution decreases in the order V > II > I > IV > III. This order is in agreement with the values of E_{imm} in HCl. When E_{imm} is more positive, the resistance to dissolution in HCl becomes more higher.

Figure 9 presents the potential-time curves for the pre-oxidized electrodes in molten $NaNO_3$ under golvanostatic anodic polarization conditions at 400°C. The plots in figure 9 indicates the presence of the induction period before dissolution of oxide scales in HCl solution. This induction period for the electrodes is shorter than under open-circuit conditions.

After the induction period the corrosion potential shifts in the active direction indicating the dissolution of the oxide scales. After this shift in potential, an arrest starts to appear on the curves, the length of which depends on the composition of the electrode. After this

arrest the potential shifts in the active direction with a rate depending on the composition of the electrode until reaching a steady-state.

The general features of the plots in figure 9 indicate the presence of multilayered oxide scales on the electrode surfaces, prompting us to calculate two dissolution rates for each electrode. The initial and final potentials for each step were deduced from the shape of curve.

The rate of dissolution for each step is also determined. It can be mentioned that time for the first step was calculated from the end of induction period to the start of arrest, the second time was calculated from the end of arrest to the starts of the steady-state.

The results of these calculations listed in TABLE 8 indicate that the outer layer of oxide scales is less protective and tends to dissolve in the acid solution, whereas the inner layer of oxide scales has a higher resistance to dissolution, the rates of dissolution of both oxide layers decreases in the order V>II>I>IV>III.

CONCLUSIONS

Electrodes I to V undergo spontaneous passivation in molten $NaNO_3$ as indicated by the open-circuit potential, galvanic current, and impedance measurements.

The passivation of the electrodes is due to the formation of surface oxide scales, formed by reaction of oxide ions with the metallic surface.

The thickness of the oxide scales increases with increasing immersion time until a steady-state is reached. The rate of thickening depends on the composition of the electrode and increases in the order V<II<I<IV< III.

The oxide scales on the electrode surfaces dissolve in aqueous HCl after an induction period which increases in the order V < II < I < IV < III.

The oxide scales formed on the electrode surfaces during anodic polarization are multilayered. The inner layer is more protective than the outer layer.

REFERENCES

[1] J. A.Gonzalez, E.Ramirez, V.Lopez, S.Flores; Plat. Surf.Finish., **10**, 54 **(1994)**.

[2] S.M.Lee, S.I.Pyun; J.Appl.Electrochem., **22**, 151 **(1992)**.

[3] S.Morisaki, H.Nagase; Jpn.Surf.Finish.Soc., **45**, 1152 **(1994)**.

[4] S.Morisaki, Y.Oguwa, T.Maeno, C.Yonezawa, Y.Ito, H.Sawahata; Jpn.Surf.Finish.Soc., **47**, 456 **(1996)**.

[5] H.H.Shih, S.L.Tzou; Surf.Coating Tech., **124**, 278 **(2000)**.

[6] S.Gudic, J.Radosevic, M.Kliskic; J.Appl.Electro chem., **26**, 1027 **(1996)**.

[7] C.A.Melendres, S.Van Gils, H.Terryn; Electrochemistry Communi-Cations, **3**, 737 **(2001)**.

[8] R.K.Nigan, R.Kapoor; Indian.J.Chem., **16A**, 7424 **(1978)**.

[9] G.David, T.A.Keith; Brit.Uk.Pat Appl.G.B., 2, 986, 855 (Cl. C25D 11/04) **(1979)**.

[10] I.I.Manukhina, V.I.Sanniknov, B.B.Antenov; Rasplavy, **4**, 58 **(1996)**.

[11] H.A.Abdel-Hakim, A.A.Attia, A.N.Al-Masri, A.M. Baraka; Anti-Corrosion Methods and Materials, **48**, 99 **(2001)**.

[12] H.A.Adbel-Hakim. A.A.Attia, A.M.Baraka; J.Mat. Engng.Perf., **11**, 301 **(2002)**.

[13] A.A.Attia, H.A.Abdel-Hakim, A.N.Al-Masri, A.M. Baraka; Mat.Wiss.u.Werkstoffech, **30**, 1 **(1999)**.

[14] H.Lux; Z.Elekrochem, **45**, 303 **(1939)**.

[15] H.Lux; Z.Elektrochem, **52**, 220 **(1948)**; **53**, 43 **(1949)**.

[16] H.Flood, T.Forland, K.Motzfeldt; Acta Chim. Scand., **6**, 257 **(1952)**.

[17] A.G.gad-Allah, H.A.Abd-El-Rahman; Corrosion NACE, **43**, 689 **(1987)**.

[18] A.G.gad-Allah, H.A.Abd-El-Rahman, M.M.Abou-Romia; Br.Corros.J., **23**, 181 **(1988)**.

[19] S.A.Salih, A.N.El-Masri, A.M.Baraka; J.Mat.Sci., **36**, 1 **(2001)**.

[20] T.Bunzo, O.Takoe; Hyomen Gijutu, **43**, 233 **(1992)**.

[21] S.A.Salih, A.N.El-Masri, A.M.Baraka; J.Mat.Sc., **36**, 2547 **(2001)**.

[22] A.A.Attia, S.A.Salih, A.M.Baraka; Electrochim. Acta, **48**, 113 **(2002)**.

[23] Q.W.Walter; Corros.Sci., **26**, 681 **(1986)**.

[24] M.Azzi, J.J.Romeau; Corros.Sci., **30**, 439 **(1990)**.

[25] W.A.Badawy, F.M.Al-Kharafi; Corros.Sci., **37**, 681 **(1997)**.

[26] F.M.Kharafi, W.A.Badawy; Electrochim.Acta, **42**, 579 **(1997)**.

[27] F.Mansfeld, M.W.Kending, S.Tsai; Corrosion, **37**, 301 **(1981)**.

[28] F.Mansfeld., M.W.Kending, S.Tsai; Corrosion, **38**, 570 **(1982)**.

[29] R.Delevie; Electrochim.Acta, **10**, 113 **(1965)**.

[30] M.Metikos-Hukovic, R.Bobic, Z.Gwabac, S.Brinic; J.Appl.Electrochem, **24**, 772 **(1994)**.

[31] T.Tsurs, S.Haruyama; Boshoku, Gijutsu; J.Japan Soc.Corros.Engng., **27**, 573 **(1978)**.